

Batch fabrication of carbon nanotube bearings

A Subramanian¹, L X Dong¹, J Tharian², U Sennhauser² and B J Nelson^{1,3}

¹ Institute of Robotics and Intelligent Systems, ETH Zurich, 8092 Zurich, Switzerland

² Electronics/Metrology Laboratory, EMPA, 8600 Dübendorf, Switzerland

E-mail: bnelson@ethz.ch

Received 30 October 2006, in final form 1 December 2006

Published 12 January 2007

Online at stacks.iop.org/Nano/18/075703

Abstract

Relative displacements between the atomically smooth, nested shells in multiwalled carbon nanotubes (MWNTs) can be used as a robust nanoscale motion enabling mechanism. Here, we report on a novel method suited for structuring large arrays of MWNTs into such nanobearings in a parallel fashion. By creating MWNT nanostructures with nearly identical electrical circuit resistance and heat transport conditions, uniform Joule heating across the array is used to simultaneously engineer the shell geometry via electric breakdown. The biasing approach used optimizes process metrics such as yield and cycle-time. We also present the parallel and piecewise shell engineering at different segments of a single nanotube to construct multiple, but independent, high density bearings. We anticipate this method for constructing electromechanical building blocks to be a fundamental unit process for manufacturing future nanoelectromechanical systems (NEMS) with sophisticated architectures and to drive several nanoscale transduction applications such as GHz-oscillators, shuttles, memories, syringes and actuators.

S Supplementary data are available from stacks.iop.org/Nano/18/075703

(Some figures in this article are in colour only in the electronic version)

1. Introduction

Supermolecular bearings based on inter-shell displacements in MWNTs have been demonstrated to be ultra-fast, fatigue-free constructs with very low friction [1–3]. Apart from their favourable nanomechanical performance, the variation of NT resistance with telescoping core motion [4] provides a unique mechanism to electrically sense and control their operation. These electromechanical building blocks can be used to create tubular switches [5–7], memories [8], nano-servomotors with integrated position sensing [9], resonators/oscillators [10, 11], and rotational elements for use in NEMS [12, 13].

The native MWNT geometry consists of nested cylinders of carbon atoms that are closed at both ends. This geometry needs to be selectively modified with control over

location, length and shells in order to create structures where some shells can axially translate or rotate with respect to others. The most commonly used methods to create nanotube bearings include electrically controlled vaporization of shells [6, 10, 13] and mechanical shell destruction, either by manipulation [9, 14] or electrostatically actuated metal paddles [12, 15]. Of these techniques, current-driven shell engineering [16–20] is more promising since it is simpler, provides better control over breakdown location and can realize fundamental architectures suited for diverse nanoscale devices. In this method, electrically induced Joule heating causes high NT temperatures [16, 17, 19, 21, 22], which are estimated to be as high as 2000 K. High resolution imaging of an individual NT inside a TEM [16, 21] has shown that at these elevated temperatures, defects such as kinks and holes are initiated at MWNT mid-lengths and result in individual shell removal in the region between contacting electrodes

³ Author to whom any correspondence should be addressed.

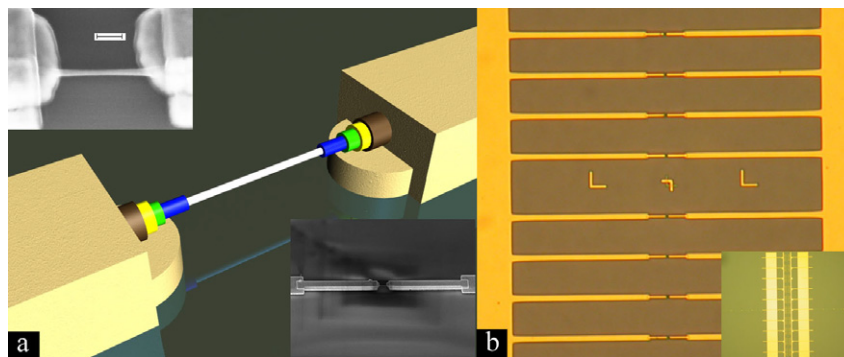


Figure 1. Nanostructure and array design. (a) Schematic diagram of the MWNT nanostructure. SEM images of the nanostructure at high and low magnification are provided in the top-left and bottom-right insets, respectively. The scale bar in the top-left inset represents 100 nm. (b) Nanoelectrode array design. A lower magnification image in the inset shows the entire array.

with associated drops in current. Though prototype bearings and devices built using this method have recently proven concepts [6, 10, 13], the capability to modify the structure of MWNTs in parallel represents an important challenge towards their eventual manufacturability and commercialization. Here, we have scaled this barrier and demonstrated that the current-driven breakdown technique, using a novel biasing approach to ensure high-yield and low cycle-time, can engineer suitably designed MWNT nanostructures in parallel to create arrays of bearings with different architectures.

2. Results

2.1. MWNT nanostructure and array overview

The primary requirement for simultaneously engineering an array of NTs, while applying a common electrical bias, is that the MWNT-based nanostructures are created with nearly identical electrical circuit resistance and heat transport conditions. This causes uniform Joule heating across the array and etches all nanotubes in parallel to fabricate bearings. In addition, the nanostructure should lend itself towards location and shell-selective alteration of MWNT geometry. A schematic of such a nanostructure and the typical array design is shown in figures 1(a) and (b). The nanostructure consists of a MWNT bridging two nanoelectrodes at its distal ends while remaining fully suspended and flat in the region between them. The NT is sandwiched between two layers of metal at each end to improve electrical contact. With this architecture, the metallic contacts serve as heat sinks, and shell removal due to thermal stress occurs in the suspended segment, as shown in figure 1(a). Also, the nature of contact with lithographically patterned electrodes ensures that etching proceeds from the outermost to inner shells.

The fabrication process used to build the nanostructure array is as follows. The bottom nanoelectrode layer (15 nm Cr/45 nm Au) is first defined on a silicon substrate, which is covered with an insulating 500 nm oxide. The nanoelectrode layer is formed by defining patterns in a bi-layer resist (PMMA/P(MAA)) using electron beam lithography, followed by metal deposition and lift-off. The electrodes are designed with 300 nm widths and separated by 350 nm gaps. Arc grown MWNTs, which are suspended in ethanol, are assembled

onto the nanoelectrodes using dielectrophoretic (DEP) forces generated by a composite AC–DC electric field [23, 24]. Next, a top metal layer of 15 nm Cr/45 nm Au is deposited to form the nanostructure array. Finally, these MWNT-nanostructure arrays are engineered using the electric breakdown technique in air and the results are investigated using SEM imaging.

2.2. Biasing approach and process control

Robust bearing operation with low-friction requires that at least 5–10 outer shells are etched in each NT of the array [13]. We find that the threshold bias for removing these shells in an array is spread over a 300–600 mV range (from V_{TH-low} to $V_{TH-high}$), which we refer to as the ‘array breakdown spectrum’. Two factors contribute to this spread in threshold bias. Within a NT, each shell has a characteristic breakdown bias that increases from the outer to inner shells [25]. In addition, the breakdown bias varies from one nanotube to the other over a small range due to possible differences in contact conditions and NT properties such as diameter or chirality.

Since applying a voltage that is much higher than the array breakdown spectrum causes the destruction of all NT shells in a single step, precise determination of the lowest voltage where breakdown is initiated at one or more NTs, V_{TH-low} , is important. Some efforts have reported that shell breakdown in single NTs occurs at the current saturation limit associated with backscattering by optical phonons and, hence, have determined the threshold voltage by measuring the $I-V$ profile of the MWNT [20]. However, we have observed such saturation in only two cases from more than 25 experiments involving individual NTs, NT arrays and parallel transport through multiple segments of single NTs. This absence of saturation has also been reported previously [16, 18], where it has been attributed to a shift in the saturation bias beyond breakdown threshold in NTs with large diameters and short lengths. In arrays, the onset of saturation in some NTs being masked by others in the $I-V$ plots can also be not ruled out.

In the absence of saturation, the only way to precisely determine $V_{TH,low}$ involves starting with a very low bias (~ 1.5 V) and progressively increasing the bias in successive cycles with small increments until breakdown is initiated. After the initiation of breakdown, the electric stress is repeatedly applied within the breakdown spectrum to structure

all the NTs. With more than 20 biasing cycles typically required for structuring arrays, the duration and voltage profile used for each of these biasing cycles impacts on process metrics such as yield and cycle-time. We find that applying the breakdown voltages for short timescales of the order of tens of milli-seconds accelerates the shell structuring process without compromising its controllability. This compares favourably with the continuous application of the breakdown bias over longer duration cycles [16–18], where we find time intervals between shell removal to be of the order of hundreds of seconds (see supplementary online material for direct comparison (available at stacks.iop.org/Nano/18/075703)).

The voltage profile used within the short duration biasing cycles has a direct influence on the process yield. A profile that sweeps voltages from 0 to V_{\max} provides higher yields than approaches that start with a high bias, such as constant bias pulses or sweeps from $-V_{\max}$ to V_{\max} . In this report, this is demonstrated using results from two NT arrays, labelled ‘A1’ and ‘A2’. In array ‘A1’, electric stress is applied by sweeping voltages from $-V_{\max}$ to $+V_{\max}$ in 10 mV increments and 100 μs time steps. We refer to this as a ‘biasing cycle’ or simply ‘cycle’. I_0 is defined as the magnitude of current at $-V_{\max}$. We start with a V_{\max} value of 1.5 V, and slowly increase it by 100 mV in each successive cycle. With the initiation of breakdown, the biasing cycle for each V_{\max} is repeated several times until there is no further shell breakdown at that voltage. It is important to note that with each successive cycle at the same V_{\max} , contact annealing increases conductance [19], while shell breakdown reduces conductance. Thus, the measured value of I_0 is impacted by contributions from these two competing components. Initially, for a given V_{\max} , the drop in current due to shell removal is higher than contact annealing and results in decreasing I_0 with each cycle. However, after all shells with the breakdown threshold corresponding to V_{\max} have been vaporized, contributions from contact annealing can be observed. Thus, an unchanging or increasing value for I_0 during successive cycles indicates complete breakdown of all shells with that threshold voltage. We subsequently increase V_{\max} by 100 mV in the next biasing cycle. We define an electric breakdown control parameter, called the current ratio (ΔI_0)%, as $((I_{0,\text{high}} - I_{0,\text{low}}) \times 100) / I_{0,\text{high}}$ and use it to track the shell breakdown process. We find that a current ratio value ranging from 30 to 35% represents an appropriate shell engineering termination point where partial shell removal occurs at all NTs. Except for using voltage sweeps from 0 to V_{\max} , the biasing procedure for array ‘A2’ is identical to that of ‘A1’.

2.3. Shell engineering results for array ‘A1’

In this array, 12 NTs formed structures suited for controlled shell engineering, as illustrated in figure 1(a). Of these nanotubes, we were able to form eight bearings which are shown in figures 2(a)–(g). It can be seen that the NTs are thinnest at the centre, with termination of thinning occurring near the contacts. The breakdown occurring at the centre shows that electrical transport through nanotubes is diffusive. In addition, the variation in threshold voltages is evident from the fact that the extent of thinning is different in different nanotubes. Two more nanotubes were fully broken and one of these is shown in figure 2(h). The remaining two nanotubes

appear to be partly thinned. However, as shown in figure 2(i), the thinning is not symmetric about the axis of these tubes, and it is not clear if these can be used as bearings.

In addition, there were 13 more NTs in this array that contributed to electric currents but were not suited for controlled shell engineering due to imperfections such as structural kinks, two overlapping tubes or contact with only one metal layer at one of their ends. Nanotubes, representative of different types of structural imperfections at these 13 locations, are shown in figures 2(j)–(l). The full breakdown summary of all NTs can be found in figure 2(m). We find that two thirds of the nanotubes that had a structure suited for controlled engineering, as illustrated in figure 1(a), form bearings (8 out of 12). It is important to note that the yield estimate for electric breakdown technique excludes the remaining 13 NTs. This is justified since the structural imperfections that make these NTs unsuitable for controlled shell engineering were caused by steps in the nanofabrication process prior to electric breakdown. For instance, nanotubes that are in contact with only the bottom metal layer and are not covered by the top metal layer on one side exhibit breakdown near that contact since most of the power is dissipated there (due to higher contact resistance).

The array transport behaviour before the onset of electric breakdown (figure 3(a)) is similar to previously published measurements from single nanotubes [16, 19] and exhibits a linear, ohmic characteristic at low bias. However, the conductance increases at high bias due to increasing contributions from the inner shells (via tunnelling currents), which are not in physical contact with the electrodes. This is shown in the inset of figure 3(a). The array breakdown spectrum was found to occur in the 2.4–2.8 V range and the variation in I_0 with successive biasing cycles, after the onset of breakdown, is shown in figure 3(b). A total of 28 biasing cycles were used and the current ratio is computed as 32%, with I_0 ranging from a high of 5.138 mA (cycle #5) to a low of 3.493 mA (cycle #28). The typical nature of individual I – V plots can be seen in the five successive biasing cycles from -2.8 to $+2.8$ V shown in figure 3(c). Since most of the individual current steps due to shell etching are much lower ($<100 \mu\text{A}$) than the magnitude of currents (~ 3.5 mA at V_{\max} of 2.8 V), the changing currents with successive cycles can be better discerned from the high bias regions shown in figures 3(d) and (e). We find that shell breakdown always occurs only at the high bias parts of each cycle. This is evident from the current reduction occurring only in the first and last 10 mV regions of the cycle from $-V_{\max}$ to $+V_{\max}$. In addition, there are a few step increases in current, as seen in cycle #27 of figure 3(d). We believe that these are due to self-healing of defects, which brings a shell back into the conduction pathway of a MWNT. This argument is supported by the appearance and disappearance of defects as well as defect migration during breakdown, as observed by Huang *et al* [16].

2.4. Failure mode analysis and process optimization

The complete breakdown of some nanotubes in a single step is an important failure mode that reduces the yield of partly etched nanotubes for use as bearings. In array ‘A1’, two of the 12 perfect NTs (and 5 of 25, overall) were fully broken.

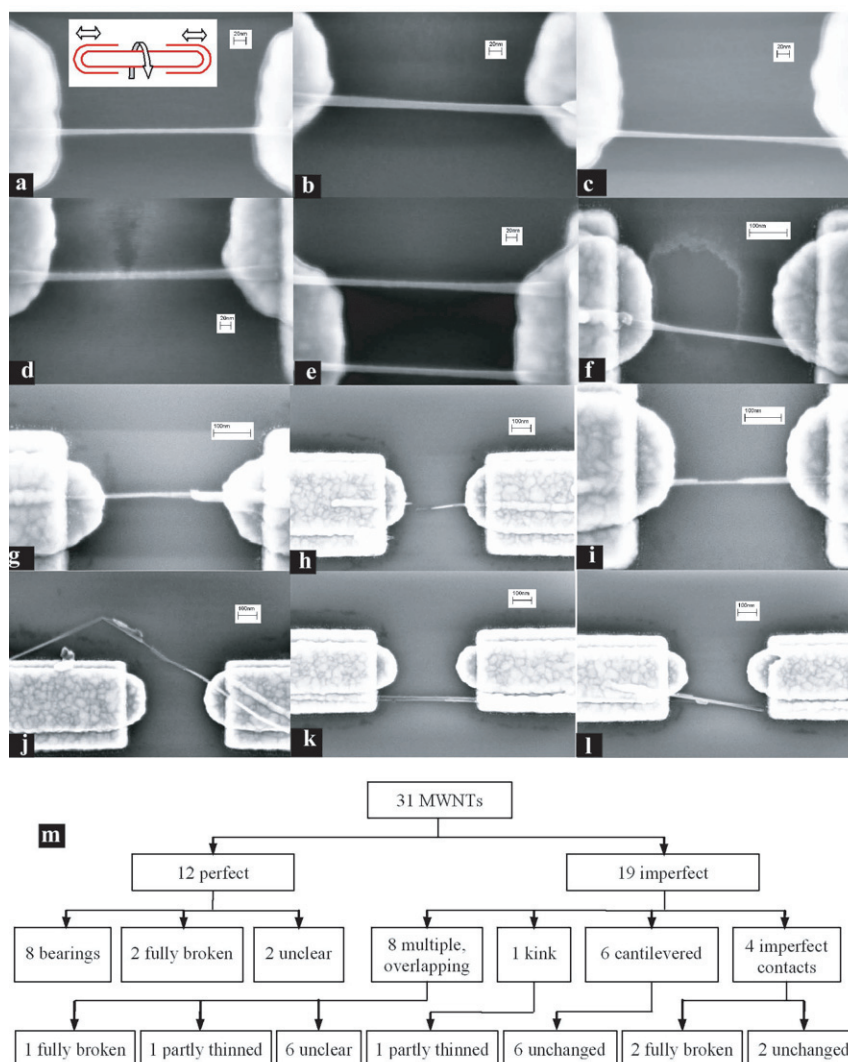


Figure 2. Batch fabrication results for array ‘A1’. (a)–(g) Bearings created by partial electric breakdown. Nanotube thinning in the region between electrodes is clearly visible. Also, the possible degrees of freedom for the engineered nanotubes are shown in the inset of panel (b). (h) Fully broken nanotube with two segments. (i) Partly thinned nanotube, where the breakdown appears to be partial and asymmetric about the core. This may or may not be a bearing. (j) NT with a kink that is partly thinned. (k) Nanotube with improper contacts. (l) Two overlapping nanotubes. The scale bars represent 20 and 100 nm in panels (b)–(f) and (g)–(m), respectively. (m) Full summary of the array.

We believe that this is caused by using a biasing scheme that starts with a high bias. This argument is supported by large drops in current at the start of a few cycles. In ‘A1’, there is a $844 \mu\text{A}$ drop at -2.5 V in cycle #5, as can be seen in figure 3(f). The high bias at the start of the cycle might result in voltage overshoots, before stabilization of the source meter at the set-point, and results in complete or substantial shell breakdown. Since a biasing cycle that uses $-V_{\text{max}}$ to $+V_{\text{max}}$ sweeps effectively applies a high bias pulse at the beginning of the cycle, it is evident that this failure mode is an issue with short duration, constant voltage biasing cycles as well.

Using a biasing profile that sweeps the voltage from 0 to V_{max} prevents this failure mode and improves the process yield. This can be seen from the results of array ‘A2’, where eight of nine nanotubes formed partly thinned bearings as shown in figures 4(a)–(h), while breakdown at the ninth nanotube could not be clearly verified within the resolution limits of SEM imaging. The imperfect tubes in this array

were removed from the circuit prior to electric breakdown, as shown in figure 4(i), by disconnecting electrode lines using focused ion-beam (FIB) machining. The array breakdown spectrum for a current ratio of 33.1% occurred over 1.8 to 2.1 V. The variation of I_0 (defined as current at V_{max}) with biasing cycles and representative I – V plots showing current steps can be seen in figures 4(j) and (k), respectively. As seen in figure 4(k), the individual current steps are $<30 \mu\text{A}$ and single-step breakdown of whole NTs does not occur with this method, resulting in a high process yield of 89%.

2.5. Piecewise engineering of individual nanotubes

Finally, we present the piecewise and parallel modification of shell structures at different segments along the length of a MWNT. This is a powerful tool for realizing bearings with more complex architectures and for forming multiple devices on a single NT leading to ultra-high density NEMS. We achieve

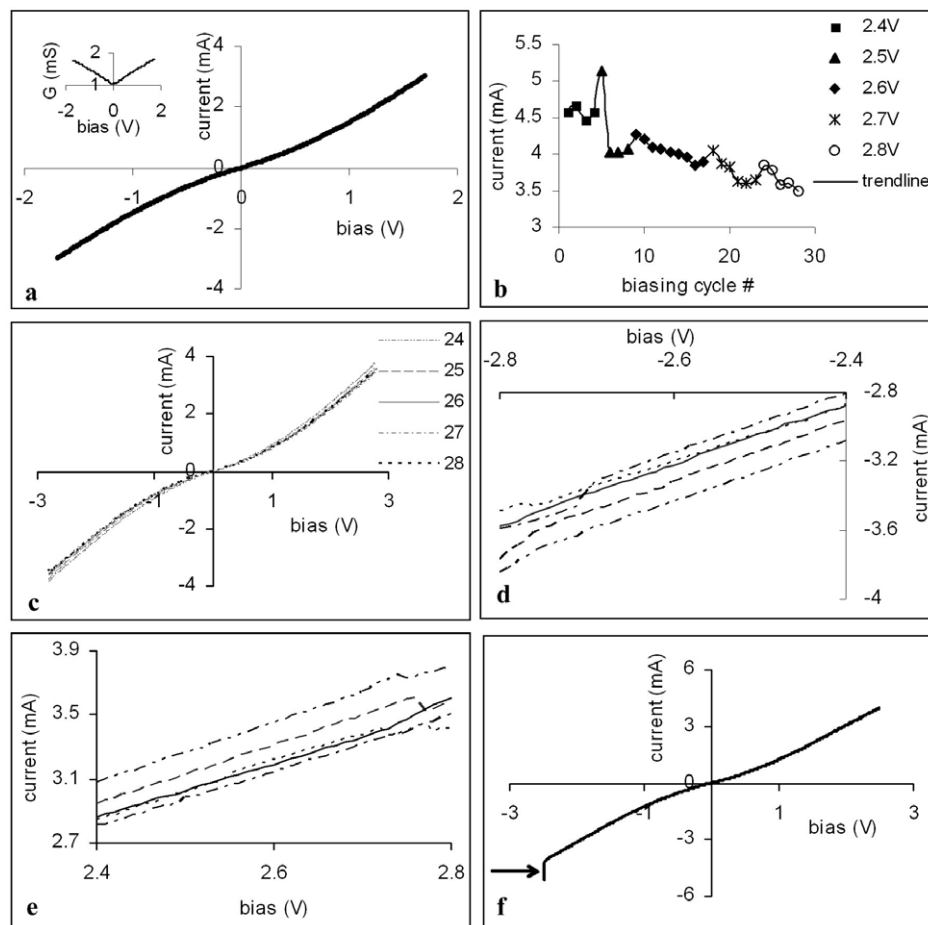


Figure 3. Electrical measurements during shell structuring of array 'A1'. (a) I - V plots before the onset of shell breakdown; increasing conductance with bias can be seen in the inset. (b) Variation of I_0 with biasing cycles. I_0 reduces during successive cycles at the same V_{\max} and increases during the transition from one voltage level to the next higher level. (c) I - V plots measured during biasing cycles 24 to 28 are shown. (d) A closer view of the negative, high bias region of cycles 24 to 28. (e) A closer view of the positive, high bias region of cycles 24 to 28. Current reduction and shell breakdown occurring primarily within these high bias segments are evident from panels (d) and (e). (f) The breakdown of entire NTs in a single step at the start of cycle 5 is shown in this plot. The arrow points to the 844 μ A drop in current that occurs at -2.5 V.

this with suitable electrode designs for DEP assembly and current-driven shell etching steps. A nanotube bridging three electrodes is schematically shown in figure 5(a), and an SEM image of the array is shown in the inset. By applying a common potential to the electrodes at distal ends and grounding the central metal contact (figure 5(a)), we can simultaneously drive currents through both suspended segments of the NT and remove its outer walls in parallel. A nanotube engineered using this technique has an architecture that is different from those illustrated in figures 2 and 4. One such NT and its shell structure with possible degrees of freedom are shown in figure 5(b).

We can realize higher bearing densities by assembling NTs onto a larger number of spatially separated electrodes with appropriate designs. Figures 6(a)–(c) show independent NT bearings with a 220 nm pitch created at different locations along the length of a single MWNT bridging five electrodes. Figure 6(a) illustrates how the alternate metal contacts are held at the same potential to simultaneously drive currents through every suspended segment and etch outer shells in parallel. The nanostructure array is shown in the inset of this figure. Also,

the peeling of outer walls in every segment of the NT is clearly visible in figures 6(b) and (c), where the left and right portions of this structure are highlighted separately. Even though the extent of thinning is different at different segments of the tube, this should not impact on bearing operation.

If we break all shells in one step, instead of partial thinning, we can create five telescoping segments with a 220 nm pitch, separated by ~ 6 –15 nm gaps as shown in figure 6(e). Each of these NT segments is anchored to the metal at only its outer shells. Hence, we now have bi-directional linear bearings with inner shells capable of sliding inside the outer housing. A schematic illustration of the nanostructure, with the inter-segment gaps exaggerated to reveal the shell architecture, is shown in figure 6(f). This is an interesting structure with a number of potential applications. With extremely small lengths (about 210 nm) for the three segments in the middle, these should exhibit lower friction forces and faster response times during telescoping core movements than previously reported [6]. With the core free to slide in either direction, these segments can be used as

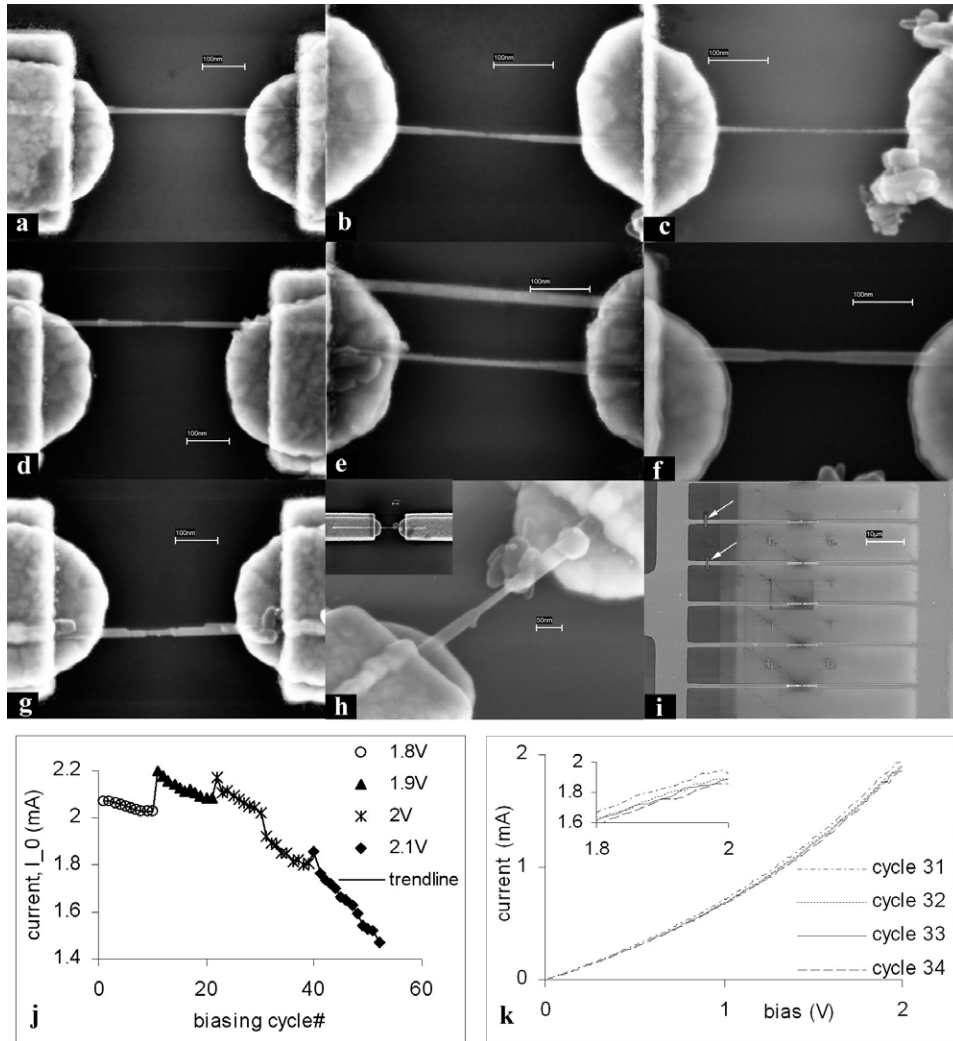


Figure 4. Batch fabrication results for array 'A2'. (a)–(h) Bearings created by partial electric breakdown. The NT on the top in panel (e) does not show any visible thinning within the resolution limits of the SEM and hence, it is not clear if this will operate as a bearing. Also, panel (h) shows the NT imaged with a stage tilt of 40° and it can be clearly seen that the polyhedral carbon nanoparticle is beneath the NT without affecting its topology. The top view of this NT is shown in the inset in this image. (i) Schematic diagram of the nanoarray design with arrows pointing to FIB machined breaks on the electrode layer. The imperfect nanotubes on these electrodes were thus removed from the electric breakdown circuit. (j) Variation of I_0 with successive biasing cycles. (k) Individual I – V plots for cycles 31 to 34 illustrating the gradual reduction in currents. The inset shows a closer view of the high bias regions. The scale bars represent 100 and 50 nm in panels (a)–(g) and (h), respectively. The scale bar in panel (i) represents 10 μm .

oscillators where neighbouring nanotube segments electrically excite oscillations.

We estimate the oscillation frequency of the three telescoping segments in figure 6(e) that can exhibit core motion on both sides using the model derived by Zheng *et al* [26, 27]. Since the NT is engineered using a single step breakdown, the lengths of all shells are nearly equal and the frequency is given as

$$f_0 = \frac{1}{4} \sqrt{\frac{\Pi}{2m\eta l_c \Delta}} \quad (1)$$

where Π represents the cumulative van der Waals interaction energy between an atom in each shell comprising the core and all the atoms of outer shells, m is the mass of a carbon atom (19.93×10^{-27} kg), l_c is the core length (210 nm) and Δ is the initial extrusion of the core. The presence of multiple shells

in the core is accounted for by a dimensionless parameter η , which is defined as

$$\eta = \left(1 - \frac{(n_c - 1)g}{d}\right) n_c \quad (2)$$

where n_c is the number of shells in the telescoping core, g is the inter-shell spacing of 0.34 nm and d is the core diameter. For a telescoping core of diameter 10 nm, the van der Waals interaction energy between the four shells located on either side of the interface between the core and outer shells can be obtained as $\Pi = 8.59 \times 10^{-21}$ J. Even though we estimate the core and outer casing to have 14 shells each, the shells that are situated further away from the interface contribute very little to the van der Waals forces and have hence, been neglected in determining Π . Thus, we compute the oscillation frequency for a 5 nm initial core extrusion using equations (1) and (2) to be 1.28 GHz.

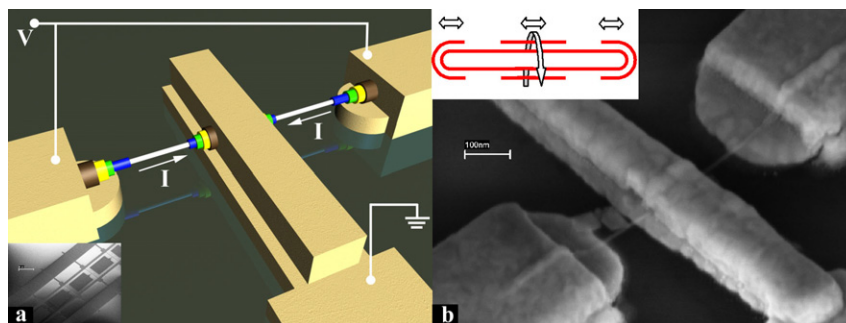


Figure 5. Formation of a nanobearing with a different architecture via piecewise engineering of single NTs. (a) Illustration of a MWNT assembled by floating electrode DEP. The electrode wiring scheme for parallel shell structuring is also shown. The inset shows an SEM image of the fabricated array at a tilt of 40° with the scale bar representing $50 \mu\text{m}$. (b) SEM image of a nanobearing formed by this method shown at a stage tilt of 40° , with the scale bar representing 100 nm . The inset illustrates the degrees of freedom of the NT shell structure.

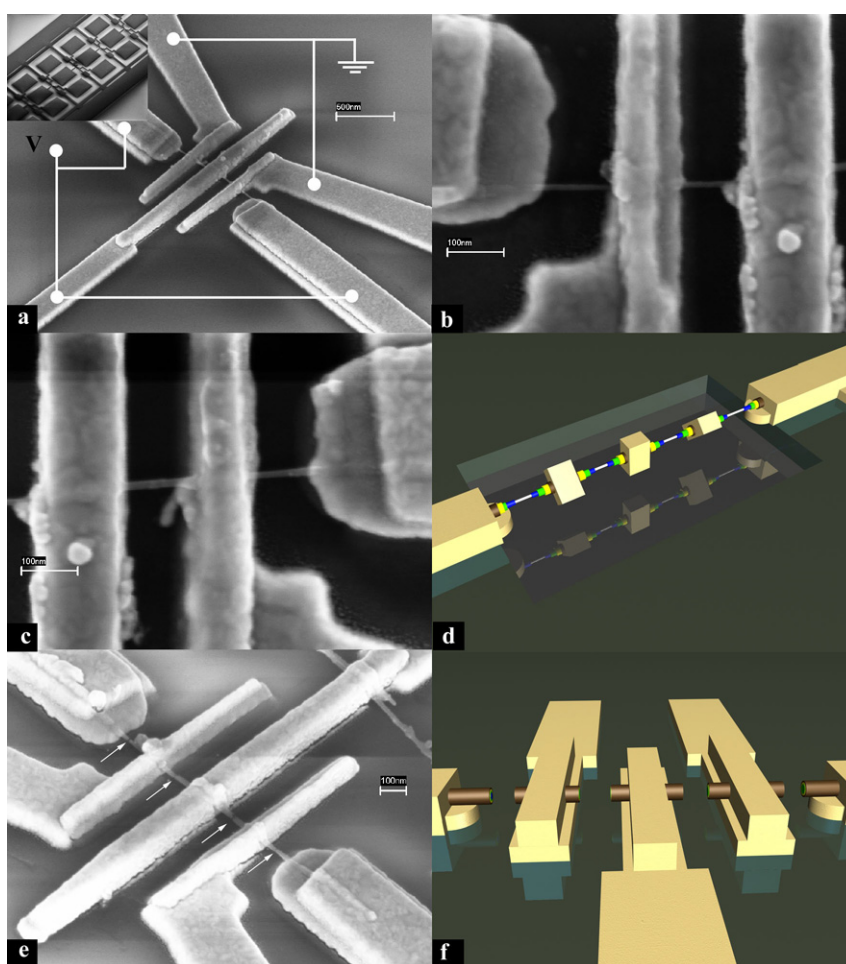


Figure 6. High density NT bearings. (a) MWNT assembled onto five spatially separated metallic contacts and thinned in the regions between contacts. The electrode wiring scheme for current-driven engineering is also shown. The array design can be seen in the top-left inset. (b), (c) High magnification SEM images clearly showing outer shell removal in all segments of this NT. (d) Schematic illustration of high density MWNT rotary motors and independent bearings that can be created by further nanomachining of this structure. (e) Telescoping segments formed with a 220 nm pitch and separated by $\sim 6\text{--}10 \text{ nm}$ gaps. The arrows point to the inter-segment gaps in this image taken with a stage tilt of 40° . (f) Schematic illustration of the core-shell mechanisms formed in panel (e) with the inter-segment gaps exaggerated to reveal the shell structure. The scale bars represent 500 nm in panel (a) and 100 nm in panels (b), (c) and (e).

It is important to note that we have assumed all shells with diameters below 10 nm extrude together as a single core. However, unlike in Zhang *et al*'s report [26, 27],

the caps on both sides of our core are open leading to the possibility of only a few intermediate shells extruding with two sliding interfaces between the moving/stationary shells.

In the case of two sliding interfaces, the retraction energies and oscillation frequencies will be higher and, hence, our estimate of 1.28 GHz based on a single sliding interface is conservative. Our models indicate that the precise shells that extrude are determined by the energetic stability of the shell configuration and the magnitude/profile of the externally applied extruding force. A comprehensive analysis of the stable shell configurations and their oscillation frequency spectrum will be presented elsewhere. It is important to note that this is the first successful fabrication of bi-directional core-shell mechanisms which have been modelled extensively [26–30], and the suitability of our technique for batch fabrication further enhances the significance of this result. Another possible application of this structure is for electromechanical switches and non-volatile memories based on inter-segment gap closing by electrostatically attracted cores [6, 7]. We are currently investigating the performance characteristics of these structures with initial results pointing to core actuation at voltages between 1 and 6 V.

3. Discussion

An important attribute of the bearing fabrication process is the short cumulative cycle-time of the order of a few seconds (array 'A1' required 28 biasing cycles of <60 ms each, while 'A2' required 52 cycles of <25 ms each). This represents an efficiency of three to four orders of magnitude in time over an approach that applies the breakdown bias continuously over longer durations. For our arrays, the longer duration biasing method consistently requires individual biasing cycles lasting 200–400 s, resulting in process times of a few hours for an array requiring at least 20 cycles. It is important to note that the breakdown timescales, using the same biasing technique in single nanotubes, has varied from several seconds to several hundreds of seconds in previous reports [16–20] and our measurements lie within this range.

We attribute this faster shell etching rate to the 'thermal shock' associated with the repeated short duration biasing cycles where rapid changes in NT temperatures accelerate the defect generation and shell removal process. During a sweep from 0 to V_{\max} in <25 ms, NT temperatures rapidly increase with the bias due to Joule heating before cooling down at the end of the cycle. We estimate the time constant for nanotubes to attain thermal equilibrium with changing bias to be approximately 4.9 ns (see supporting online material for computation (available at stacks.iop.org/Nano/18/075703)). This is much lower than the 100 μ s time steps for voltage increments in our biasing schemes and supports the argument that heat dissipation in NTs is fast enough to follow changes in applied electrical bias. With cycle times of a few tens of milliseconds, rapid cycling of temperatures accelerates the defect formation in NT shells and results in faster breakdown. We have also directly verified this difference in breakdown timescales between the long and short biasing time methods. This was accomplished by removing the outermost shells of an array of two nanotubes using short duration biasing cycles. Then, the subsequent shells were found to etch at the same power, but at a much slower rate, by applying a constant bias with longer duration. The results from this experiment unambiguously confirm our conclusions

and are provided as supporting online material (available at stacks.iop.org/Nano/18/075703).

4. Conclusions

We have successfully demonstrated the batch fabrication of nanoscale bearings using dielectrophoretically assembled MWNTs. The biasing approach used results in bearing formation by electric breakdown with high-yield and low cycle-time. In addition, this technique lends itself to create sophisticated MWNT shell architectures and high density bearings. Due to its compatibility with conventional silicon micro/nanomachining steps, further processing can create more complex nanostructures. This robust method to form fundamental electromechanical building blocks is expected to enable the manufacturability and commercialization of next generation NEMS.

References

- [1] Cumings J and Zettl A 2000 *Science* **289** 602
- [2] Kolmogorov A N and Crespi V H 2000 *Phys. Rev. Lett.* **85** 4727
- [3] Kis A, Jensen K, Aloni S, Mickelson W and Zettl A 2006 *Phys. Rev. Lett.* **97** 025501
- [4] Cumings J and Zettl A 2004 *Phys. Rev. Lett.* **93** 086801
- [5] Forro L 2000 *Science* **289** 560
- [6] Deshpande V V, Chiu H Y, Postma H W C, Miko C, Forro L and Bockrath M 2006 *Nano Lett.* **6** 1092
- [7] Yan Q M, Zhou G, Hao S G, Wu J and Duan W H 2006 *Appl. Phys. Lett.* **88** 173107
- [8] Maslov L 2006 *Nanotechnology* **17** 2475
- [9] Dong L X, Nelson B J, Fukuda T and Arai F 2006 *IEEE Trans. Autom. Sci. Eng.* **3** 228
- [10] Jensen K, Girit C, Mickelson W and Zettl A 2006 *Phys. Rev. Lett.* **96** 215503
- [11] Kang J W, Song K O, Kwon O K and Hwang H J 2005 *Nanotechnology* **16** 2670
- [12] Fennimore A M, Yuzvinsky T D, Han W Q, Fuhrer M S, Cumings J and Zettl A 2003 *Nature* **424** 408
- [13] Bourlon B, Glatli D C, Miko C, Forro L and Bachtold A 2004 *Nano Lett.* **4** 709
- [14] Yu M F, Jakobson B I and Ruoff R S 2000 *J. Phys. Chem. B* **104** 8764
- [15] Yuzvinsky T D, Fennimore A M, Kis A and Zettl A 2006 *Nanotechnology* **17** 434
- [16] Huang J Y, Chen S, Jo S H, Wang Z, Han D X, Chen G, Dresselhaus M S and Ren Z F 2005 *Phys. Rev. Lett.* **94** 236802
- [17] Molhave K, Gudnason S B, Pedersen A T, Clausen C H, Horswell A and Boggild P 2006 *Nano Lett.* **6** 1663
- [18] Lee Y H, Lee J H, Chung S J, Lee S and Ju B K 2006 *Appl. Phys. Lett.* **89** 073109
- [19] Yuzvinsky T D, Mickelson W, Aloni S, Konsek S L, Fennimore A M, Begtrup G E, Kis A, Regan B C and Zettl A 2005 *Appl. Phys. Lett.* **87** 083103
- [20] Collins P G, Hersam M, Arnold M, Martel R and Avouris P 2001 *Phys. Rev. Lett.* **86** 3128
- [21] Chen S, Huang J Y, Wang Z, Kempa K, Chen G and Ren Z F 2005 *Appl. Phys. Lett.* **87** 263107
- [22] Kuroda M A, Cangellaris A and Leburton J P 2005 *Phys. Rev. Lett.* **95** 266803
- [23] Lu S N, Chung J and Ruoff R S 2005 *Nanotechnology* **16** 1765
- [24] Subramanian A, Vikramaditya B, Dong L X, Bell D J and Nelson B J 2005 *Robotics: Science and Systems I* ed S Thrun *et al* (Cambridge, MA: MIT Press) pp 327–34
- [25] Bourlon B, Glatli D C, Placais B, Berroir J M, Miko C, Forro L and Bachtold A 2004 *Phys. Rev. Lett.* **92** 026804

- [26] Zheng Q S and Jiang Q 2002 *Phys. Rev. Lett.* **88** 045503
- [27] Zheng Q S, Liu J Z and Jiang Q 2002 *Phys. Rev. B* **65** 245409
- [28] Guo W L, Guo Y F, Gao H J, Zheng Q S and Zhong W Y 2003 *Phys. Rev. Lett.* **91** 125501
- [29] Rivera J L, McCabe C and Cummings P T 2003 *Nano Lett.* **3** 1001
- [30] Legoas S B, Coluci V R, Braga S F, Coura P Z, Dantas S O and Galvao D S 2003 *Phys. Rev. Lett.* **90** 055504

NANOTECHNOLOGY

VOLUME 18 NUMBER 7 21 FEBRUARY 2007



www.iop.org/journals/nano

Featured article:

Batch fabrication of carbon nanotube bearings
*A Subramanian, L X Dong, J Tharian, U Sennhauser
and B J Nelson*